NASA/TM—2016-218939

Time-Dependent Stress Rupture Strength Degradation of Hi-Nicalon Fiber-Reinforced Silicon Carbide Composites at Intermediate Temperatures

Roy M. Sullivan
Glenn Research Center, Cleveland, Ohio

January 2016

NASA STI Program . . . in Profile

Since its founding, NASA has been dedicated to the advancement of aeronautics and space science. The NASA Scientific and Technical Information (STI) Program plays a key part in helping NASA maintain this important role.

The NASA STI Program operates under the auspices of the Agency Chief Information Officer. It collects, organizes, provides for archiving, and disseminates NASA's STI. The NASA STI Program provides access to the NASA Technical Report Server—Registered (NTRS Reg) and NASA Technical Report Server—Public (NTRS) thus providing one of the largest collections of aeronautical and space science STI in the world. Results are published in both non-NASA channels and by NASA in the NASA STI Report Series, which includes the following report types:

- TECHNICAL PUBLICATION. Reports of completed research or a major significant phase of research that present the results of NASA programs and include extensive data or theoretical analysis. Includes compilations of significant scientific and technical data and information deemed to be of continuing reference value. NASA counter-part of peer-reviewed formal professional papers, but has less stringent limitations on manuscript length and extent of graphic presentations.

- TECHNICAL MEMORANDUM. Scientific and technical findings that are preliminary or of specialized interest, e.g., "quick-release" reports, working papers, and bibliographies that contain minimal annotation. Does not contain extensive analysis.

- CONTRACTOR REPORT. Scientific and technical findings by NASA-sponsored contractors and grantees.

- CONFERENCE PUBLICATION. Collected papers from scientific and technical conferences, symposia, seminars, or other meetings sponsored or co-sponsored by NASA.

- SPECIAL PUBLICATION. Scientific, technical, or historical information from NASA programs, projects, and missions, often concerned with subjects having substantial public interest.

- TECHNICAL TRANSLATION. English-language translations of foreign scientific and technical material pertinent to NASA's mission.

For more information about the NASA STI program, see the following:

- Access the NASA STI program home page at http://www.sti.nasa.gov

- E-mail your question to help@sti.nasa.gov

- Fax your question to the NASA STI Information Desk at 757-864-6500

- Telephone the NASA STI Information Desk at 757-864-9658

- Write to:
  NASA STI Program
  Mail Stop 148
  NASA Langley Research Center
  Hampton, VA 23681-2199

Time-Dependent Stress Rupture Strength Degradation of Hi-Nicalon Fiber-Reinforced Silicon Carbide Composites at Intermediate Temperatures

Roy M. Sullivan
Glenn Research Center, Cleveland, Ohio

National Aeronautics and
Space Administration

Glenn Research Center
Cleveland, Ohio 44135

January 2016

Acknowledgments

Level of Review: This material has been technically reviewed by technical management.

Available from

Time-Dependent Stress Rupture Strength Degradation of Hi-Nicalon Fiber-Reinforced Silicon Carbide Composites at Intermediate Temperatures

Roy M. Sullivan
National Aeronautics and Space Administration
Glenn Research Center
Cleveland, Ohio 44135

Abstract

The stress rupture strength of silicon carbide fiber-reinforced silicon carbide (SiC/SiC) composites with a boron nitride (BN) fiber coating decreases with time within the intermediate temperature range of 700 to 950 °C. Various theories have been proposed to explain the cause of the time-dependent stress rupture strength. The objective of this paper is to investigate the relative significance of the various theories for the time-dependent strength of SiC/SiC composites. This is achieved through the development of a numerically-based progressive failure analysis routine and through the application of the routine to simulate the composite stress rupture tests. The progressive failure routine is a time-marching routine with an iterative loop between a probability of fiber survival equation and a force equilibrium equation within each time step. Failure of the composite is assumed to initiate near a matrix crack and the progression of fiber failures occurs by global load sharing. The probability of survival equation is derived from consideration of the strength of ceramic fibers with randomly occurring and slow growing flaws as well as the mechanical interaction between the fibers and matrix near a matrix crack. The force equilibrium equation follows from the global load sharing presumption. The results of progressive failure analyses of the composite tests suggest that the relationship between time and stress-rupture strength is attributed almost entirely to the slow flaw growth within the fibers. Although other mechanisms may be present, they appear to have only a minor influence on the observed time-dependent behavior.

Introduction

The stress rupture strength of silicon carbide fiber-reinforced silicon carbide (SiC/SiC) composites with a boron nitride (BN) fiber coating is time dependent within the intermediate temperature range of 700 to 950 °C. The strength of these composites in the fiber direction under constant stress loading conditions decreases with time. Alternatively, one may view this behavior as a time delayed failure, where the time-to-failure is inversely proportional to the applied stress magnitude.

This time-dependent strength behavior is illustrated by the experimental data plotted in Figure 1, which was originally published in Morscher, Hurst and Brewer (Ref. 1). Figure 1 contains fast fracture strength data at 815 °C and stress rupture strength data at 815 and 880 °C. The data was obtained in tests performed on Hi-Nicalon fiber-reinforced, melt infiltrated silicon carbide composites. The material was reinforced with a 5HS woven fabric, with a tow spacing of 17 ends per inch (epi). Each tow contained 500 fibers, with an average fiber radius of 7 μm. The tests were performed on flat dog-bone specimens which were 8 plies thick. The arrow on one of the stress rupture data points in Figure 1 signifies that this specimen did not fail. This test was interrupted at the time indicated before failure occurred.

The time-dependent strength of SiC/SiC composites in the intermediate temperature range has been the topic of many previous studies. Various theories have been proposed to explain the cause of the time-dependent stress rupture strength (Refs. 1 to 11). A common theme among all proposed strength-limiting mechanisms is that they are all enabled by an oxidation reaction that is expected to occur at a sufficient rate within the intermediate temperature range of 700 to 950 °C.
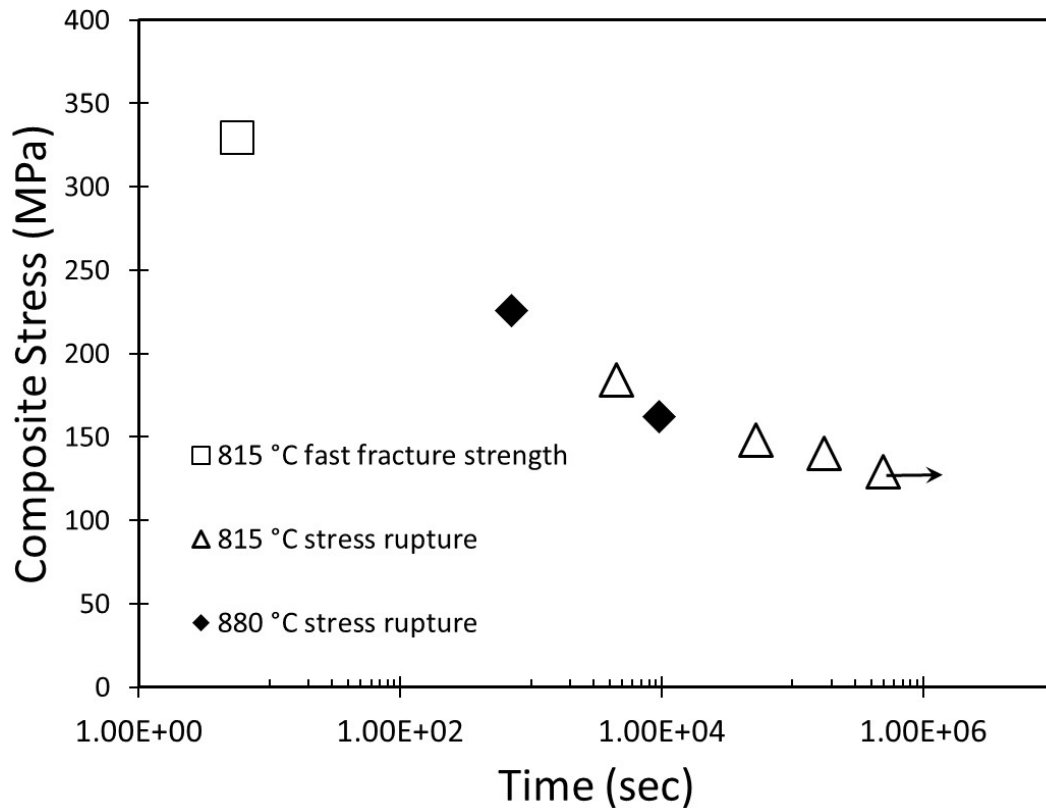
Figure 1.—Stress versus time-to-failure of Hi-Nicalon composite specimens at intermediate temperatures. Data from Morscher, Hurst and Brewer (Ref. 1).

A number of researchers (Refs. 1 to 7) attribute a time-dependent loss of strength to the oxidation of the BN fiber coating. The oxidation of the BN coating and the formation of silica at the interface causes the fibers to fuse to the matrix and to one another. They argue that failure of any of the fused fibers will result in a stress concentration in the nearest intact fiber, making it more likely that the nearest neighbor will also fail. This results in a cascading of fiber failures and failure of the composite cross-section at a stress value significantly lower than the fast fracture strength. This proposition is consistent with a time-dependent strength degradation, since the process of oxidation and fiber fusing takes time and the extent to which the cross-section is *embrittled* will increase with time. As such, one would expect the stress rupture strength of the composite to decrease with time.

More recently, Xu, Zok and McMeeking (Ref. 8) have suggested two other possible mechanisms which could be responsible for the loss of composite strength over time. The first involves oxidation of the SiC fibers and the second involves oxidation of the fibers or matrix within a matrix crack. Regarding the first, they have suggested that the growth of a silica scale on the fiber surface induces a tensile stress in the fibers. The tensile stress is generated by the difference in the molar volumes of SiC and SiO_2. Under the second scenario, oxide growth within a matrix crack can act as a wedge which pries the matrix crack open. This also induces a tensile stress in the crack bridging fibers. In both scenarios, the tensile stress in the fibers increases with time since the magnitude of the tensile stress is a function of the amount of oxide growth. The difference between the inherent strength of the SiC fibers and the oxide growth-induced tensile stress results in the apparent strength reduction over time.

A third group of authors (Refs. 9 to 11) propose that the observed composite strength behavior is due to an inherent time-dependent strength degradation of the fibers and that the cause of the fiber strength degradation is the slow growth of flaws within the fibers. They contend that slow flaw growth within the fibers is facilitated by oxidation of either SiC or the free carbon at the grain boundaries. These authors were influenced by the previous work of Davidge, et al. (Ref. 12), who recognized the effect of flaws on the time-

dependent and stochastic strength in ceramic materials and who established a three-way relationship between stress, time and the probability of failure. Based upon this previous work, Gauthier and Lamon (Ref. 11) developed a similar three-way relationship for Hi-Nicalon, Hi-Nicalon Type S, and Nicalon fibers.

The objective of this paper is to investigate the relative significance of the various theories for the time-dependent strength degradation of SiC/SiC composites. This is achieved through the development of a numerically-based progressive failure analysis routine and through the application of the routine to simulate the composite stress rupture tests which produced the results in Figure 1. The progressive failure routine assumes that the progression of fiber failures occur by global load sharing. Failure of the composite is assumed to initiate near a matrix crack, as this is the location where the fibers carry the highest stress and likely have the highest probability of failure.

The progressive failure analysis solution is based on an iterative solution between an equation for the probability of survival of the reinforcing fibers and an equation of force equilibrium within each time step. Both equations were derived from consideration of the mechanical interaction between the fibers and the matrix near a matrix crack (Refs. 13 to 19). The equation of force equilibrium is obtained from the work of Thouless and Evans (Ref. 15) and Curtin, et al. (Ref. 18). The progressive failure analysis of the composite is similar to the analysis described in Halverson and Curtin (Ref. 19), except herein the analysis is performed numerically and the formulation of the probability of fiber survival equation follows from the triadic relation between stress, time and probability of failure for ceramic fibers provided by Gauthier and Lamon (Ref. 11).

The progressive failure analyses presented in this paper neglect the effects of BN fiber coating oxidation and the resulting fiber fusing and local load sharing. They neglect to include the effect of oxide scale growth either within the matrix cracks or on the fiber surfaces and the resulting stress that develops in the bridging fibers. The only time-dependent strength-limiting mechanism included in the progressive failure analyses is that proposed by Lamon and his coworkers (Refs. 9 to 11), which results from the time-dependent growth of flaws within the fibers. Comparison of the results obtained by the progressive failure analysis to the measured behavior shown in Figure 1 reveals the significance of the slow flaw growth effect. By this comparison, one may also judge the significance of the other strength-limiting mechanisms proposed by the previous authors.

Fiber Failure Model (Relationship Between $P_f - \sigma - t$)

The strength of ceramic fibers is limited by the presence of flaws either within the fibers or on the surface of the fibers. Fiber failure occurs when the stress intensity factor equals the fracture toughness K_{Ic}. The stress intensity factor is given by $K_I = \sigma_f\, Y\sqrt{C}$, where σ_f is the average stress in the fiber, C is the size of the critical flaw and Y is a unit-less geometrical parameter, which has a specific value for each flaw shape. Thus, the fast fracture strength of the fiber, denoted as σ_f^s, is related to the initial flaw size C_i according to

$$C_i = \left(\frac{K_{Ic}}{\sigma_f^s Y} \right)^2 \tag{1}$$

In stress rupture tests, the combination of the applied stress magnitude and initial flaw size are typically not large enough to result in immediate fiber failure. However, over time the flaws will slowly propagate under the fiber stress σ_f. At some point, one of the flaws will reach a sufficient size to satisfy the failure criteria, $K_I = K_{Ic}$. The time-to-failure is the time it takes a flaw to grow from its initial size C_i to the critical size under the fiber stress σ_f. Previous authors (Refs. 9 to 11) claim that the slow growth of flaws in SiC fibers is enabled by oxidation at the fiber grain boundaries.

Davidge, et al. (Ref. 12) developed an expression for the time-to-failure of ceramic materials, subjected to an applied stress σ. They assumed that the flaw growth velocity is a function of the stress intensity factor according to $v = dC/dt = \alpha_1 K_I^n$, where α_1 and n are flaw growth parameters, and obtained the following expression for the relation between the applied stress σ, the initial flaw size C_i and time-to-failure t:

$$\sigma^n t = \frac{2 C_i^{(2-n)/2}}{\alpha_1 Y^n (n-2)} \tag{2}$$

Equation (2) may also be applied to ceramic fibers. A plot of t versus σ_f obtained from stress rupture tests performed on a group of single fibers, all with an identical initial flaw size and shape, will lie along a curve defined by $\sigma_f^n t = A$, where A is a constant.

Both the fast fracture fiber strength and the product $\sigma_f^n t$ are stochastic quantities since they depend on the initial size of randomly occurring flaws on or within the fibers. It is not practical to obtain the flaw size distribution in a population of fibers. However, the nature of the statistical distribution of initial flaw sizes can be obtained from Equation (1) and the statistical treatment of the fast fracture strength. To this end, one may substitute Equation (1) into (2) and denote the applied stress σ as σ_f to obtain

$$\sigma_f^n t = \frac{2}{\alpha_1 Y^2 (n-2)} \left(\frac{\sigma_f^s}{K_{Ic}} \right)^{n-2} \tag{3}$$

The statistical nature of the fast fracture strength of ceramic fibers is usually modeled using the two-parameter Weibull strength model (Refs. 12, 14, 17, 19, and 20). In the Weibull strength theory, the cumulative probability of failure of a population of ceramic fibers is given by

$$P_f = 1 - \exp\left(-\frac{L}{L_o} \left(\frac{\sigma_f}{S_o} \right)^m \right) \tag{4}$$

where L_o is the reference length, m is the Weibull modulus and S_o is the characteristic strength of a fiber of length L_o (Ref. 17). The values of S_o and m are obtained from tensile strength tests performed on a population of individual fibers. L_o is the gage length used in the strength tests. The ratio L/L_o accounts for the length effect, i.e., the number of flaws in a length of fiber L are L/L_o times the number of flaws that occur in a length L_o.

By rearranging Equation (4), the fiber fast fracture strength may be written as a function of the cumulative probability of failure and the statistical parameters according to

$$\sigma_f^s = S_o \left(\frac{L_o}{L} \ln \frac{1}{1-P_f} \right)^{1/m} \tag{5}$$

Substituting Equations (5) into (3) leads to the following relationship between stress, time and probability of failure:

$$\sigma_f^n t = \frac{2}{\alpha_1 Y^2 (n-2)} \left(\frac{S_o}{K_{Ic}} \right)^{n-2} \left(\frac{L_o}{L} \ln \frac{1}{1-P_f} \right)^{\frac{n-2}{m}} \tag{6}$$
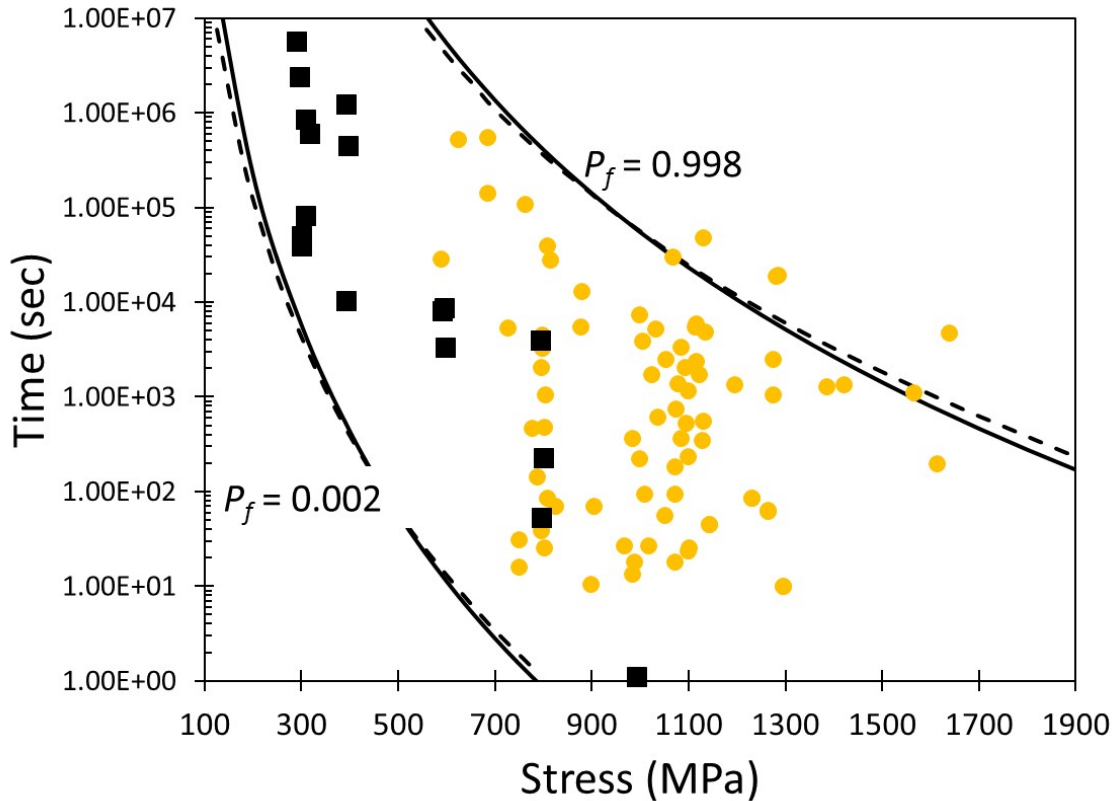
Figure 2.—Time-to-failure versus applied stress of Hi-Nicalon single fibers (gold circles) and tows (black squares) at 800 °C. Data from Gauthier and Lamon (Ref. 11).

Equation (6) includes the flaw growth parameters, the statistical fast fracture strength parameters as well as the length effect. It is very similar to the equation derived in Gauthier and Lamon (Ref. 11) except that the equation derived by the previous authors contains an additional term (Note: The parameter α_1 is denoted as A_1 in Reference 11). Gauthier and Lamon (Ref. 11) state that the additional term is insignificant under most conditions of interest and may be neglected. A form of Equation (6) will be used in progressive failure analyses of the Hi-Nicalon composite stress rupture tests in the following sections of this paper.

The time-to-failure versus applied stress reported by Gauthier and Lamon (Ref. 11) for Hi-Nicalon fibers and tows at 800 °C is plotted in Figure 2. The single fiber results are plotted as gold circles and the tow results are plotted as black squares. Figure 2 reveals the scatter in the initial flaw size and shape in Hi-Nicalon fibers, as it reveals the scatter in the product $\sigma_f^n t$. One can imagine a series of curves of the form $\sigma_f^n t = A$, each one with a different value of A and each one passing through one or more of the single fiber data points in Figure 2.

The values for the constants in Equation (6), which will be used in the progressive failure analyses, are listed in Table 1. Some of the values listed were the values listed in Table III of Gauthier and Lamon (Ref. 11) for Hi-Nicalon fibers. The rest were obtained by fitting Equation (6) to match the plots of time-to-failure versus fiber stress at specific values of the probability of failure. This is illustrated by the plots of t versus σ_f at $P_f = 99.8\%$ and $P_f = 0.2\%$ shown in Figure 2. The dashed lines are the lines from Figure 7 in Gauthier and Lamon (Ref. 11) and the solid lines are a plot of Equation (6) using the constants listed in Table 1. The plots of t versus σ_f obtained from Equation (6) and the constants in Table 1 provides a very good match to those from the previous authors. Both sets of plots encapsulate almost all of the

TABLE 1.—TABLE OF CONSTANTS FOR THE $P_f - \sigma - t$ MODEL FOR Hi-NICALON
FIBERS AT INTERMEDIATE TEMPERATURES

n	m	K_{Ic} (MPa $\cdot \sqrt{m}$)	S_o (MPa)	L_o (m)	$\alpha_1 Y^2$ (MPa$^{-n} \cdot s^{-1} \cdot m^{-(2-n)/2}$)
9	4.3	1.4	61	0.025	3.04×10^{-20}

single fiber data points from Gauthier and Lamon (Ref. 11). Note that in Table 1 the quantities Y and α_1 are not treated separately, but are accounted for by the product $\alpha_1 Y^2$. This eliminates the need to identify the shape of the flaws, since the value of the product $\alpha_1 Y^2$ is determined directly from the aforementioned treatment of the test data.

The only significant difference between the values listed in Table 1 and those suggested by Gauthier and Lamon (Ref. 11) is the value of $\alpha_1 Y^2$. The source of this discrepancy lies in the method by which the size effect is treated by the authors. The previous authors use a volume ratio V/V_o to account for the size effect and assigned the reference volume a value of $V_o = 1$ m^3. Given the length (25 mm) and radius (7.5 µm) of the single fiber tensile specimens, the volume ratio is $V/V_o = 4.4 \times 10^{-12}$. The present treatment of the experimental data assumes $L = L_o = 25$ mm. The result is a significant adjustment to the value of $\alpha_1 Y^2$. Further validation of the constants in Table 1 and the accuracy of the resulting fiber failure model will be obtained by the results of the tow tensile tests simulations discussed in the following section.

Progressive Failure Routine

A progressive failure routine was developed to simulate the progressive failure of a collection of fibers. The fibers are aligned in parallel with one another and collectively carry a total tensile load F. The progressive failure routine is performed under the assumption of global load sharing (GLS). When a fiber fails, the load it previously carried is distributed evenly to all remaining unbroken fibers. Under GLS, force equilibrium requires that the stress carried by each unbroken fiber is $\sigma_f = F/(N A_f)$, where N is the number of unbroken fibers and A_f is the area of each fiber.

For a large number of fibers, the probability of survival is approximately equal to the ratio N/N_o, where N_o is the initial number of unbroken fibers. Rearranging Equation (6) to obtain an expression for P_f in terms of σ_f and t, and recognizing $P_s = 1 - P_f$, the probability of survival may be expressed as

$$P_s = \frac{N}{N_o} = \exp\left\{ -\frac{L}{L_o}\left(\frac{\alpha_1 Y^2 (n-2)}{2} t \right)^{\frac{m}{n-2}} \left(\frac{K_{Ic}}{S_o} \right)^m \sigma_f^{\frac{mn}{n-2}} \right\} \tag{7}$$

The progressive failure routine is a time-marching routine with an iterative loop between the probability of survival and force equilibrium within each time step. The number of unbroken fibers N is calculated for the current time and current fiber stress using the probability of survival equation. An update to the fiber stress is calculated using the new value of N and the equilibrium equation. The iteration between the equilibrium and probability of survival equations occurs until convergence is obtained. When convergence is reached, time is marched forward and the process is repeated. Time-to-failure is determined numerically as the time step where solution convergence is not obtained within a large number of iterations.

A FORTRAN source code was written to implement the progressive failure routine. The solution was performed on a desktop computer.

Analysis of Tow Tests

The progressive failure routine was applied to simulate the time-dependent strength behavior in the tow tensile tests reported in Gauthier and Lamon (Ref. 11). In these tests, the time-to-failure of Hi-Nicalon and Hi-Nicalon Type S tows was measured at various constant applied stress levels and test temperatures. The analyses reported here are focused on the Hi-Nicalon tests performed at 800 °C only. The Hi-Nicalon tows contained five hundred fibers ($N_o = 500$). The constants listed in Table 1 were used as input to Equation (7).

The results of four progressive failure simulations are shown in Figure 3. The results are shown for simulations which used an initial tow tensile stress of 1100, 800, 600, and 400 MPa. The stress in the fibers is plotted in Figure 3(a) and the number of unbroken fibers is plotted in Figure 3(b). Both sets of results are plotted as a function of time. The time at which failure of the tow occurred in each of the simulations is obvious from the results in Figure 3.
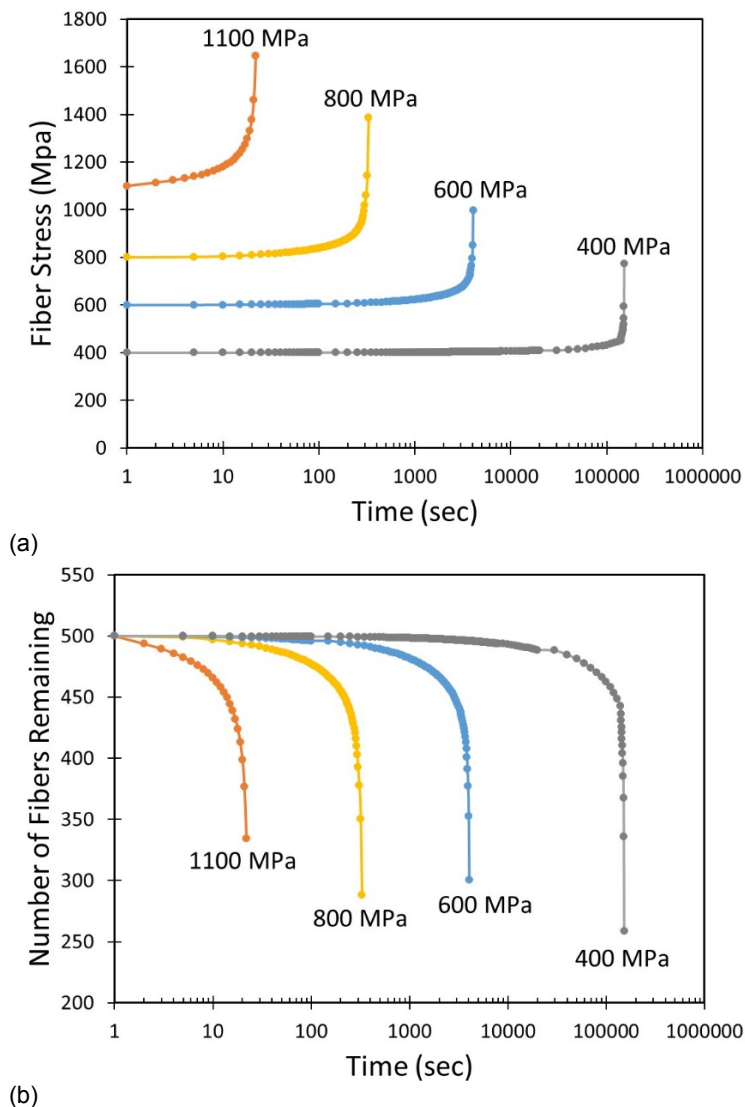

(a)

(b)

Figure 3.—Numerical results from progressive failure analysis of Hi-Nicalon tow tensile tests at 800 °C. Results are shown for numerical simulations using an initial fiber stress loading of 1100, 800, 600, and 400 MPa. (a) Fiber stress versus time. (b) Number of unbroken fibers versus time.
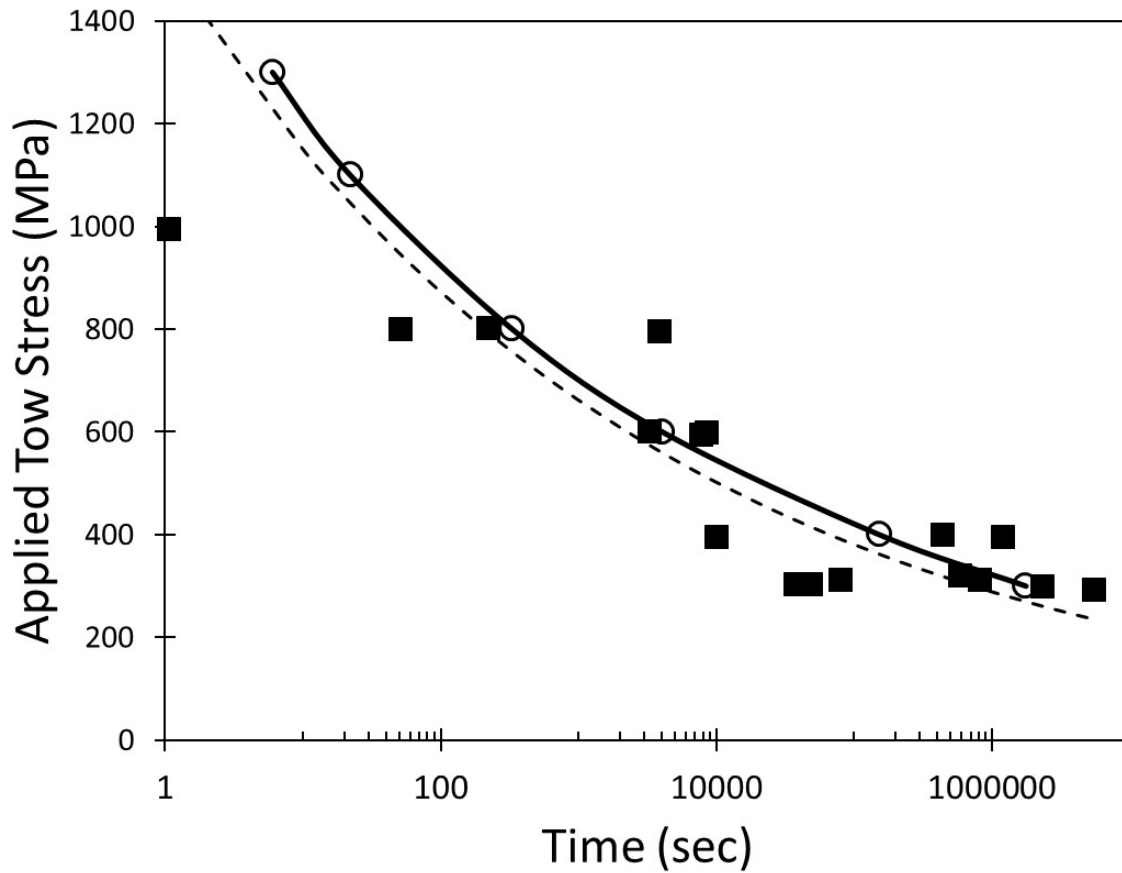
Figure 4.—Initial applied stress versus time-to-failure from tensile tests on Hi-Nicalon tows at 800 °C. Measured data from Gauthier and Lamon (Ref. 11) are shown as black squares. Dashed line is a curve-fit to the experimental data from Gauthier and Lamon (Ref. 11). Numerical results from progressive failure analysis are shown as the solid line with hollow circular markers.

Figure 4 is a comparison of the measured and predicted results from the tow tensile tests. Here the applied stress is plotted as a function of time-to-failure. The experimental measurements from Gauthier and Lamon (Ref. 11) are shown as square markers. The dashed line is a curve-fit of the experimental data using the equation $\sigma^n t = A$. The curve-fit values are $A = 3.36 \times 10^{26}$ and $n = 8.34$. These were obtained by Gauthier and Lamon (Ref. 11) using regression analysis. The progressive failure analysis results are shown as the solid black line with hollow circular markers. The results of the progressive failure simulations are in good agreement with the curve fit to the measured results provided by Gauthier and Lamon (Ref. 11). This provides a validation of the constants listed in Table 1, the resulting fiber failure model and the progressive failure analysis routine.

Analysis of Composite Failure

Mechanics at a Crack Plane

In this section, a progressive failure analysis is performed for the fibers within a composite in an attempt to predict the time-to-failure versus applied stress behavior of the composite. It is assumed that failure of the composite initiates near a matrix crack, since the fiber stresses are considerably higher near a matrix crack than in an uncracked zone. The mechanics in the vicinity of a matrix crack have been described previously by many authors (Refs. 13 to 19). Some of the basic concepts that are necessary for the current discussion will be reviewed.

Consider a collection of fibers in a composite specimen, aligned in the direction of loading and bridging a single matrix crack. Herein, the loading direction is denoted as the z direction. Over a short distance on either side of the crack plane, the fibers and matrix become de-bonded and may slip with respect to one another. Slipping is resisted by a shear stress τ acting at the fiber/matrix interface over a slip length l on either side of the crack plane. The shear stress is assumed to be constant along the slip length. At distances greater than the slip length away from the crack plane, the composite response is linear elastic with a modulus given by the rule of mixtures relation, $E = f E_f + (1-f)E_m$. The symbols E_f and E_m represent the Young's modulus of the fiber and matrix, respectively, and f is the fiber volume fraction in the direction of loading. The slip length is given by $l = (R\sigma/2\tau)(1-f)E_m / f E$, where σ is the far field composite stress and R is the fiber radius.

The fiber stress is a maximum at the matrix crack plane having a value of $T = \sigma/f$. The fiber stress decreases linearly from its maximum value at the crack plane with a slope of $2\tau/R$ reaching a value of $E_f\sigma/E$ at, and beyond, the slip length. The variation of the fiber stress within the slip length is given by $\sigma_f(z) = T - (2\tau/R)z$ where $z = 0$ at the crack plane. The matrix stress in the loading direction at the crack plane is zero. The matrix stress increases linearly with distance from the crack plane with a slope of $(2\tau/R)(f/1-f)$, reaching a maximum value of $E_m\sigma/E$ at, and beyond, the slip length.

Matrix cracking will occur at a composite stress value of σ_{mc}. At this composite stress, the stress in the matrix is $\sigma_{mc}^m = E_m\sigma_{mc}/E$. Consider now the possibility that multiple matrix cracks may form perpendicular to the direction of loading. Since the matrix stress at a crack plane is zero and increases linearly with distance from the crack plane with a slope of $(2\tau/R)(f/1-f)$, there's a length l_m on both sides of a crack, given by

$$l_m = \frac{\sigma_{mc}R}{2\tau} \frac{(1-f)E_m}{fE}, \tag{8}$$

where no additional cracks will form because the matrix stress in this length cannot reach the matrix cracking stress σ_{mc}^m. As loading is increased, cracks will continue to form until crack saturation is reached at which point the crack spacing x must satisfy $l_m \le x \le 2l_m$ (Refs. 13 and 14). The average distance between cracks at saturation is $\bar{x} = 1.337l_m$ (Ref. 21).

Probability of Survival

It is assumed that the failure of the fibers will only occur within the slip length near the crack plane so the contribution of the fiber stress outside the slip length is ignored. As previously discussed, the fiber stress varies linearly near a matrix crack and has a maximum value of $T = \sigma/f$ at the crack plane. The probability of survival of a fiber with a varying stress along its length may be obtained by dividing each fiber into Q fiber segments each of length δ_i, such that $2l = \sum_{i=1}^{Q} \delta_i$. Each fiber segment carries a different stress value σ_i depending on its distance from the crack plane. The probability of survival of a fiber is then the product of the probability of survival of all fiber segments $P_s = \prod_{i=1}^{Q} P_{s\,i}$.

The time-dependent probability of survival of a single fiber of length L under stress σ is given by Equation (7). Thus, the time-dependent probability of survival of the chain of Q fiber segments each of length δ_i carrying a stress σ_i would be

$$P_s = \prod_{i=1}^{Q} \exp\left\{ -\frac{\delta_i}{L_o}\left(\frac{\alpha_1 Y^2(n-2)}{2} t \right)^{\frac{m}{n-2}} \left(\frac{K_{Ic}}{S_o} \right)^m \sigma_i^{\frac{mn}{n-2}} \right\} \tag{9}$$

The right hand side of Equation (9) may be replaced with the mathematically equivalent form

$$P_s = \exp\left\{ -\sum_{i=1}^{Q} \frac{\delta_i}{L_o}\left(\frac{\alpha_1 Y^2(n-2)}{2} t \right)^{\frac{m}{n-2}} \left(\frac{K_{Ic}}{S_o} \right)^m \sigma_i^{\frac{mn}{n-2}} \right\} \tag{10}$$

The expression for the probability of survival is obtained by replacing the summation sign in Equation (10) with an integral and the length segments δ_i with the differential length dz and by performing the integration of the fiber stress function $\sigma_f(z)$ over the slip length. It is more convenient to approximate the fiber stress variation near the crack plane with $\sigma_f(z) = T(1-z/l)$ and to approximate the slip length as $l = TR/2\tau$ (Ref. 15). Using these approximations and upon performing the integration one obtains

$$P_s = \frac{N}{N_o} = \exp\left\{ -\frac{2l}{L_o}\left(\frac{\alpha_1 Y^2(n-2)}{2} t \right)^{\frac{m}{n-2}} \left(\frac{K_{Ic}}{S_o} \right)^m \frac{T^{\frac{mn}{n-2}}}{\left(\frac{n(m+1)-2}{n-2} \right)} \right\} \tag{11}$$

Force Equilibrium

Fibers that break a finite distance from the crack plane are capable of carrying a load at the crack plane. The stress that a broken fiber can carry at the crack plane is referred to as the pullout stress and is a function of the shear stress transferred between the fiber and matrix and the distance between the fiber fracture location and the crack plane. This distance is referred to as the pull-out length. For a single matrix crack in the gage section, force equilibrium at the crack plane requires

$$F = TNA_f + (N_o - N)A_f\langle \sigma_p \rangle \tag{12}$$

The first term in Equation (12) is the load carried by the unbroken fibers and the second term is the load carried by the broken fibers via the pullout stress. The quantity $N_o - N$ is the number of broken fibers within the slip length of the crack and $\langle \sigma_p \rangle$ is the average pull-out stress, given by $\langle \sigma_p \rangle = 2\tau\langle h \rangle / R$, where $\langle h \rangle$ is the average pull-out length. The analyses discussed in the next section utilize an equation for the average pull-out length in terms of τ, R and the statistical parameters, S_o and m, which was given in Thouless, et al. (Ref. 16). Rearranging Equation (12) leads to the following equation for the fiber stress at the crack plane under the assumption of a single matrix crack:

$$T = \frac{N_o}{N}\left[\frac{F}{N_o A_f} - \left(1 - \frac{N}{N_o}\right)\langle\sigma_p\rangle\right] \tag{13}$$

If there are multiple cracks within the specimen gage length, it is possible that the slip lengths associated with adjacent cracks may overlap. Following Curtin, et al. (Ref. 18), let us consider a crack in the matrix and designate this crack the central crack. Within the slip lengths on either side of the central crack plane there are $2l/x$ other cracks. The probability of survival (or failure) of a fiber is the same in each of the crack planes and may be calculated using Equation (11). The number of fibers that are not failed in any crack plane within the shear transfer length $2l$ of the central plane is given by $N_o - (N_o - N)(1 + 2l/x)$. These fibers carry a stress T at the central plane. The other fibers that have broken in any one of the other crack planes cannot carry a stress of T at the central plane, since there is not sufficient distance between their fracture location and the central plane. It is assumed that, on average, they carry a pull-out stress of $T/2$ at the central crack plane (Ref. 18).

Force equilibrium at the central crack plane now requires

$$F = T\left(1 - \left(1 - \frac{N}{N_o}\right)\left(1 + \frac{2l}{x}\right)\right)N_o A_f + \left(1 - \frac{N}{N_o}\right)\frac{2l}{x}\frac{T}{2}N_o A_f \tag{14}$$

The first term is the load carried by the fibers which have not failed in any crack within the slip length of the central crack plane. The second term is the load carried by the pull-out stress of the broken fibers in the vicinity of all cracks within the slip lengths of the central crack plane. Rearranging Equation (14), one obtains the following equation for the fiber stress at the crack plane if multiple matrix cracks are present:

$$T = \frac{F}{N_o A_f}\frac{1}{\left[1 - \left(1 - \frac{N}{N_o}\right)\left(1 + \frac{l}{x}\right)\right]} \tag{15}$$

Analysis Results

Progressive failure analyses were performed to simulate the progression of failure in the tensile tests performed on the Hi-Nicalon composites, reported in Morscher, Hurst and Brewer (Ref. 1). The tensile tests were performed on flat dog-bone specimens with a gage section width of 12.6 mm. The specimens were 8 plies thick, with a tow spacing of 17 epi and 500 fibers per tow. Thus, the total number of tows in the specimen gage section, in the direction of loading, was (12.6 mm/25.4)(17 epi)(8 plies) $\approx$ 67.5 tows and the number of fibers which are initially unbroken is N_o = 67.5(500) = 33,750. The thickness of 8 plies is 2.1 mm and the average fiber radius is R = 7 μm. Thus, the initial fiber volume fraction in the direction of loading is f = 0.1965.

Morscher and Cawley (Ref. 7) measured the crack density as a function of the applied composite stress for Hi-Nicalon-reinforced silicon carbide composite specimens. The crack density study was performed on a Hi-Nicalon composite similar to the test material that produced the results shown in Figure 1. The results of the crack density study by Morscher and Cawley (Ref. 7) are shown in Figure 5; the crack spacing, which is the inverse of the crack density, is plotted as a function of the composite stress. These results indicate that the matrix cracking stress is $\sigma_{mc} \approx 130$ MPa and that the matrix crack spacing at saturation is x = 0.4 mm. Given these results, and using $x = 1.337l_m$ and Equation (8), an approximate shear stress value of 5 MPa is obtained.
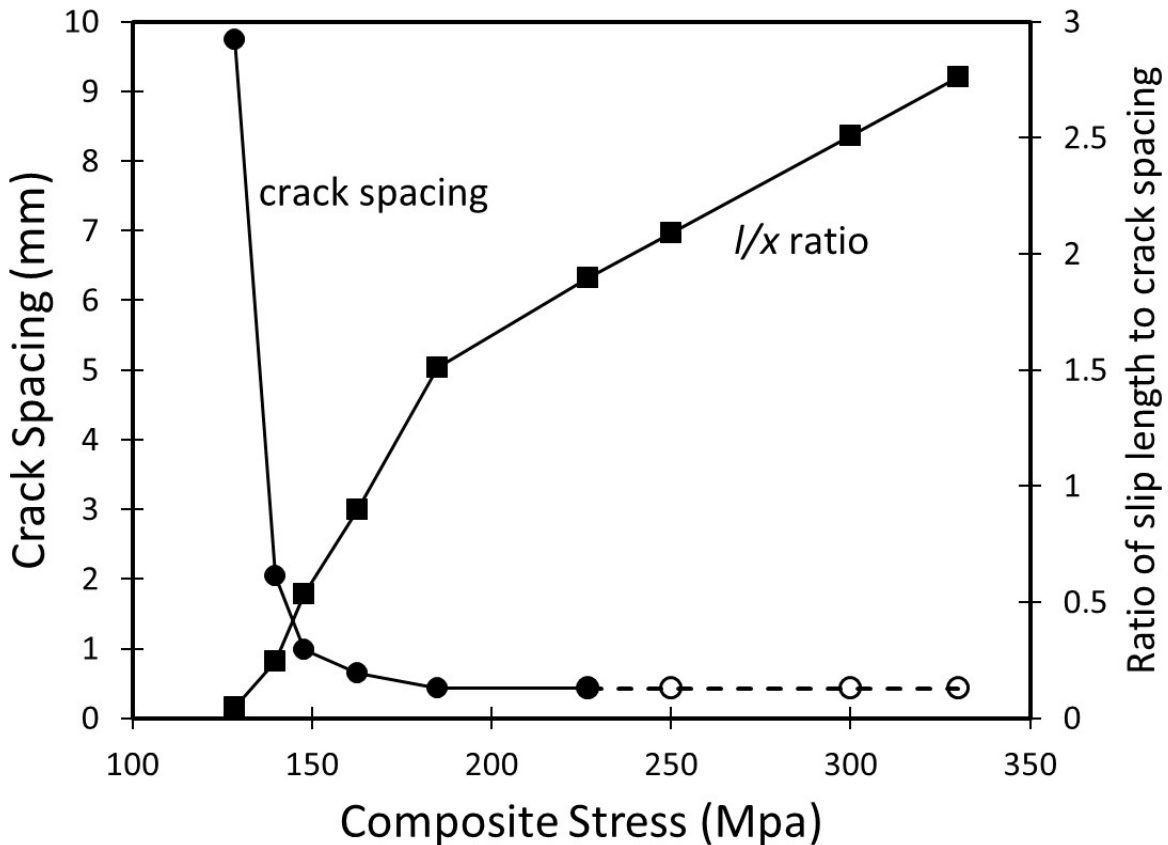
Figure 5.—Composite plot of crack spacing and ratio of slip length-to-crack spacing versus composite stress. Crack spacing versus composite stress data was obtained from crack density versus composite stress data on Hi-Nicalon composites reported in Morscher and Cawley (Ref. 7).

The choice of whether the single or multiple matrix crack equilibrium equation is more appropriate depends on the value of the ratio l/x. Equation (13) applies as $l/x \rightarrow 0$. Otherwise, Equation (15) is the more appropriate choice. The value of l/x was calculated for the range of composite stresses used in the tensile tests that produced the results shown in Figure 1. The slip length was calculated at each composite stress value from $l = TR/2\tau$ using $\tau = 5$ MPa and $R = 7$ μm. The crack spacing results obtained from Morscher and Cawley (Ref. 7) were used to calculate the ratio l/x as a function of composite stress. Note that the crack spacing data was extended to higher composite stress values since the highest stress in the crack density study by Morscher and Cawley (Ref. 7) was only 227 MPa. This is indicated with a dashed line and hollow markers in Figure 5. It was extended under the assumption that crack saturation was reached at 180 MPa. The slip length-to-crack spacing ratio is also plotted as a function of composite stress in Figure 5. Given these results, it appears that the multiple matrix crack equation of force equilibrium should be applicable for the range of composite stress values which are of interest here. For example, one would expect to have at least two other cracks within the slip length of each matrix crack at composite stress values above 160 MPa, where $l/x \geq 1$.

The progressive failure analysis simulations of the Hi-Nicalon composite tests were performed using Equation (11) for the probability of survival and either Equations (13) or (15) for the equation of force equilibrium. The time-marching scheme with iterations between the equilibrium and probability of survival equations within each time step were performed in a similar manner to that described previously. Within each time step, Equation (11) is used to obtain an update to the number of unbroken fibers N using the current time and the previous value of T. The slip length is calculated with $l = TR/2\tau$. The equilibrium equation then provides an update to the value of T. The process is repeated until convergence is reached. Time is then marched forward to the next time step.
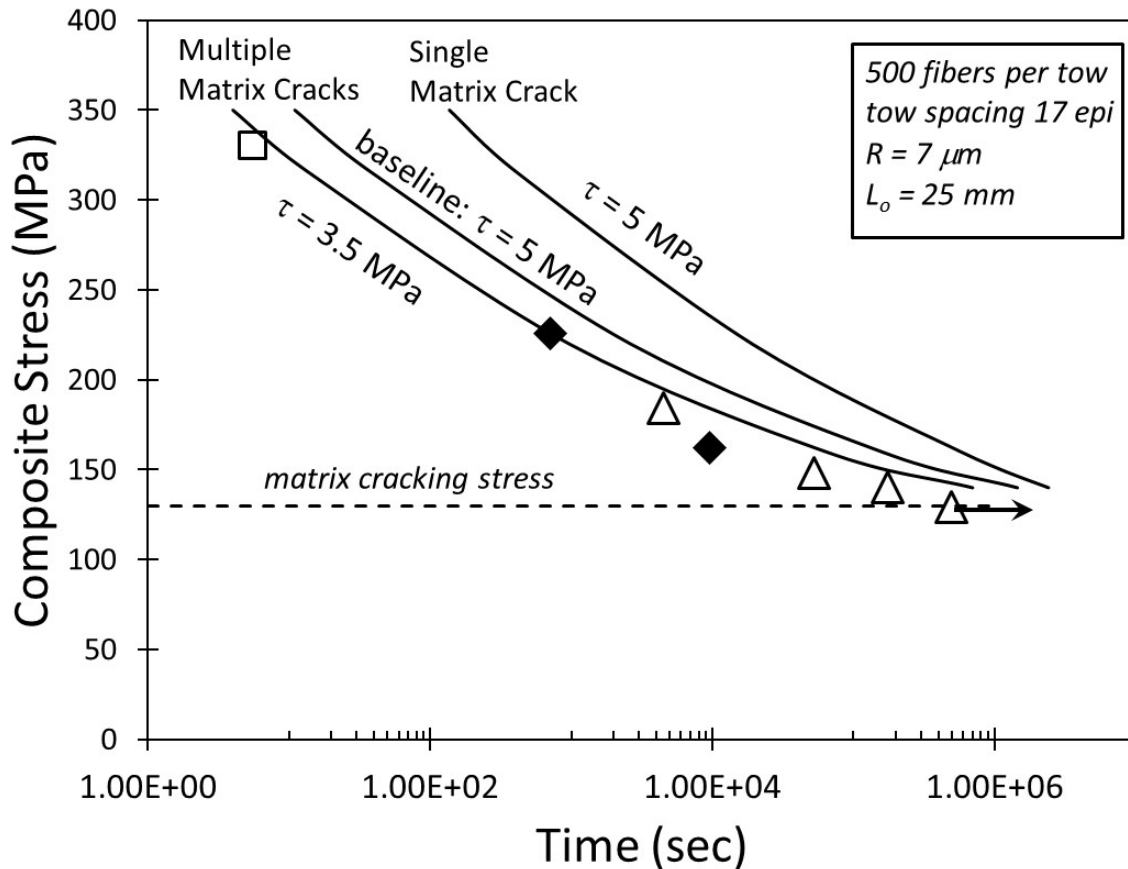
Figure 6.—Comparison of progressive failure analysis results with the experimental data from Morscher, Hurst and Brewer (Ref. 1) on Hi-Nicalon fiber-reinforced composites at intermediate temperatures. Progressive failure analysis results are shown for three series of analysis solutions: a single crack formulation (using Eq. (13) as equilibrium equation) with τ = 5 MPa, a multiple crack formulation (using Eq. (15) as equilibrium equation) with τ = 5 MPa and a multiple crack formulation with τ = 3.5 MPa.

A series of progressive failure analyses were performed for each set of solution parameters. Within each series, progressive failure analyses were performed for a variety of applied composite stress magnitudes and the time-to-failure was calculated for each stress magnitude. The results from three series of progressive failure analysis solutions are shown as the solid black lines in Figure 6. The experimental results from Morscher, Hurst and Brewer (Ref. 1) are included for comparison. One series of solutions assumed a single matrix crack and used Equation (13) as the equilibrium equation. A shear stress value of 5 MPa was used in these solutions. Another series of solutions assumed multiple matrix cracks within the gage section and used Equation (15) as the equation of force equilibrium. The ratio of l/x as a function of composite stress shown in Figure 5 was used as input to Equation (15). These solutions also used a shear stress of 5 MPa. This series of solutions will be referred to as the baseline solutions. As one would expect from the discussion of the ratio l/x in Figure 5, the results obtained using the multiple matrix crack formulation are closer to the measured results than those obtained using a single matrix crack formulation.

The baseline solutions did not produce results that were sufficiently close to the measured fast fracture strength. The progressive failure analysis method must be able to predict the fast fracture strength in order to have any expectation of predicting the composite strengths at longer times. There are a handful of possible reasons for the discrepancy between the baseline progressive failure analysis predictions and the measured fast fracture strength. One reason may be that the true shear stress between the fibers and matrix may not be exactly 5 MPa, which is the estimated shear stress value from the calculations using the crack density measurements. An additional series of progressive failure analysis solutions were

performed with the multiple matrix crack formulation and a slightly lower shear stress value. Using a lower shear stress value shifts the results either to a lower composite strength or a shorter time-to-failure, since using a lower shear stress value will result in a longer slip length and thus a lower probability of survival for the same composite stress magnitude. The results in Figure 6 show that by reducing the shear stress to a value of 3.5 MPa, there is good agreement between the predicted results and the measured fast fracture strength. Note that the value of 3.5 MPa is very close to the value obtained by Marshall and Evans (Ref. 22) for other SiC fiber-reinforced ceramic composites. They consistently obtained values in the range of 2 to 2.5 MPa using multiple techniques. Note also that, for the multiple matrix crack solutions using a shear stress value of 3.5 MPa, there is a small difference between the measured and predicted composite strengths at later times.

The matrix cracking stress has been identified with a dashed horizontal line in Figure 6. Note that the data point representing the specimen that did not fail in the tensile tests lies slightly below the matrix cracking stress value. It's not surprising that this specimen did not fail at the applied stress value, since the stress is much lower, and the probability of survival is much higher, for fibers in an un-cracked matrix than for fibers bridging a matrix crack.

Another possible reason for the discrepancy between the baseline progressive failure analysis predictions and the measured fast fracture strength may be that some of the fibers were damaged during processing. Progressive failure analyses were performed to investigate the effect of fiber damage. This was achieved by starting the progressive failure analysis simulations with a reduced initial fiber volume fraction. Progressive failure analysis results for an assumed fiber damage of 9 percent are shown in Figure 7. The experimental results from Morscher, Hurst and Brewer (Ref. 1) and the baseline solution results are included for comparison. Both sets of progressive failure simulation results shown in Figure 7 used the multiple
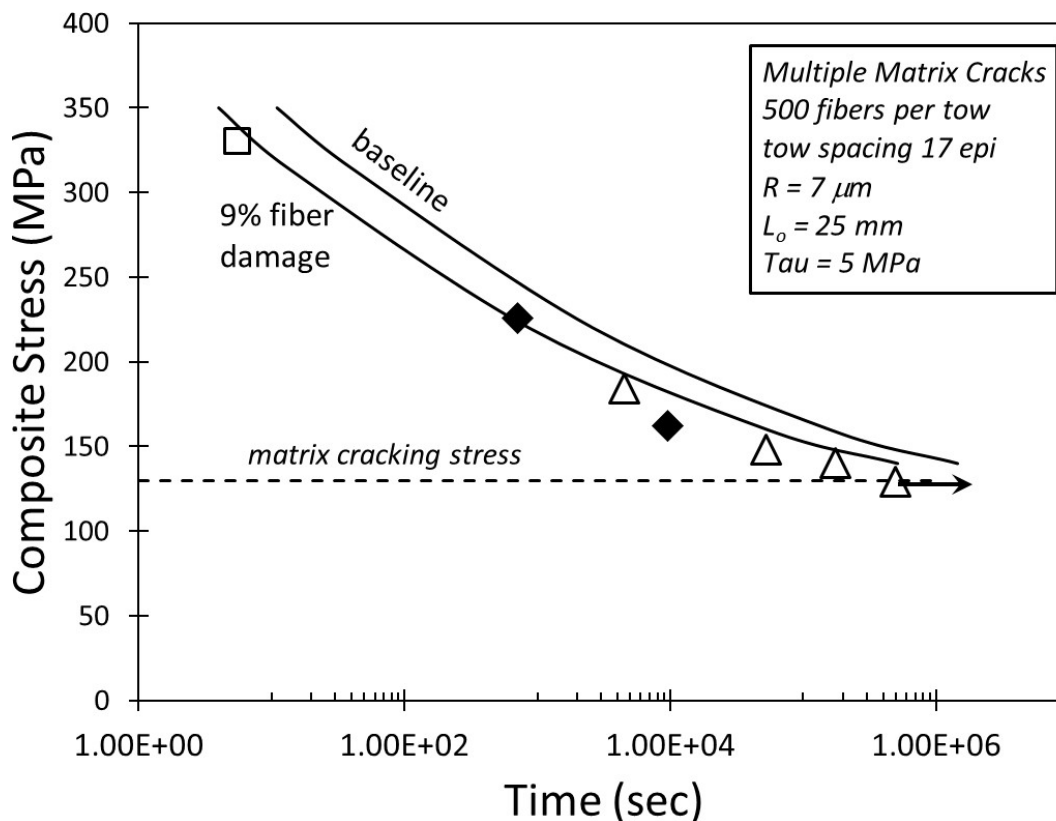

Figure 7.—Comparison of progressive failure analysis results with the experimental data from Morscher, Hurst and Brewer (Ref. 1) on Hi-Nicalon fiber-reinforced composites at intermediate temperatures. Progressive failure analysis results are shown for two series of progressive failure analysis solutions: a multiple matrix crack formulation with no fiber damage and a multiple matrix crack formulation with 9 percent fiber damage. Both sets of progressive failure analysis solutions used a shear stress value of 5 MPa.

matrix crack equilibrium equation and a shear stress value of 5 MPa. Notice that the progressive failure analysis solutions using a shear stress of 5 MPa and 9 percent fiber damage produced a very similar set of results as the solutions shown in Figure 6 that used a shear stress of 3.5 MPa and no fiber damage. In both cases, the predicted strengths are very close to the measured fast fracture strength and there is only a small difference between the measured and predicted composite strengths at later times.

A third possible reason for the discrepancy between the baseline progressive failure analysis solution results and the measured fast fracture strength may be due to the fiber architecture in the composite. Keep in mind that the progressive failure model was developed from data on straight fibers. In the composite system which is the subject of the current discussion, the reinforcement is in the form of a woven fabric. Thus, the tows are crimped (or curved) at regular intervals along the length. Applying a tensile load to curved tows results in a higher tensile stress, within the tow cross-section, than a tensile load on straight tows due to the additional stress caused by bending. If one were to account for the additional stress caused by crimped tows in the baseline progressive failure analysis, the baseline results plot would be shifted closer to the measured results. The magnitude of this shift has not yet been determined. The effect of fiber crimping on the progressive failure analysis will be left as a topic of future study.

Discussion of Results

The progressive failure analysis solutions were successful in simulating the measured relationship between time-to-failure and composite stress for a Hi-Nicalon composite tested within the intermediate temperature range. The progressive failure analysis solutions were developed under the assumption that composite failure initiated at a matrix crack and that the progression of fiber failure occurred by global load sharing. Failure of a fiber is stochastic and time-dependent due to flaws within the fiber. A model for the statistically-based and time-dependent fiber strength proposed by Gauthier and Lamon (Ref. 11) was utilized in the progressive failure analyses. No other strength-limiting mechanism, such as BN fiber coating oxidation or silica formation in a matrix crack or on the fibers, was included in the formulation. The success of the progressive failure analysis in simulating the measured relationship between time-to-failure and composite stress indicates that the time-dependent strength degradation in SiC/SiC composites at intermediate temperatures is primarily due to the intrinsic time-dependent strength of the fibers, which is the result of slow growth of flaws in the fibers.

Calculations for the ratio l/x in the Hi-Nicalon composite tests indicate that the selection of the multiple crack equilibrium equation is appropriate for these simulations. Furthermore, calculations for the shear stress using the measured crack spacing at saturation and the first matrix cracking stress reveal that the shear stress between the fibers and matrix is approximately 5 MPa. A very good match between the experimental data from Hi-Nicalon composite testing and the progressive failure analysis results was obtained using the multiple matrix crack equilibrium equation. Two sets of analysis solutions provided the best correlation with the measurements: one that used a shear stress value of 5 MPa and assumed 9 percent fiber damage and one that used a shear stress value of 3.5 MPa and assumed no fiber damage. Other combinations of shear stress and fiber damage values would provide equally favorable results. These simulations would necessarily require a shear stress value somewhere between 3.5 and 5 MPa and an assumed fiber damage less than 9 percent. These findings provide validation of the progressive failure analysis solutions, since all of these solutions require a shear stress value close to the estimated value of 5 MPa and a reasonable estimate of fiber damage.

The difference between the measured and predicted strengths at longer times may be due to the other strength-limiting mechanisms which were discussed in the introduction. However, in view of the results in Figures 6 and 7, it appears that these effects are secondary. Although the conclusions drawn here regarding the mechanisms responsible for the time-dependent strength behavior in SiC/SiC composites were based on testing and analysis of a specific composite material in a specific series of stress rupture tests, it is believed that these same conclusions apply to a wide range of SiC/SiC composites.

References

1. G.N. Morscher, J. Hurst and D. Brewer, "Intermediate-Temperature Stress Rupture of a Woven Hi-Nicalon, BN-Interphase, SiC-Matrix Composite in Air," *J. Am. Ceram. Soc.* 83 [6] 1441-49 (2000).
2. F.E. Heredia, J.C. McNulty, F.W. Zok and A.G. Evans, "Oxidation Embrittlement Probe for Ceramic Matrix Composites," *J. Am. Ceram. Soc.* 78 [8] 2097-2100 (1995).
3. G.N. Morscher, "Tensile Stress Rupture of SiCf/SiCm Minicomposites with Carbon and Boron Nitride Interphases at Elevated Temperatures in Air," *J. Am. Ceram. Soc.* 80 [8] 2029-42 (1997).
4. W.H. Glime and J.D. Cawley, "Stress Concentration Due to Fiber-Matrix Fusion in Ceramic-Matrix Composites," *J. Am. Ceram. Soc.* 81 [10] 2597-604 (1998).
5. L.U.J.T. Ogbuji, "A Pervasive Mode of Oxidation Degradation in a SiC-SiC Composite," *J. Am. Ceram. Soc.* 81 [11] 2777-84 (1998).
6. G.N. Morscher and J. Hurst, "Stress-Rupture and Stress-Relaxation of SiC/SiC Composites at Intermediate Temperature," *Ceram. Eng. Sci. Proc.*, 22 539-546 (2001).
7. G.N. Morscher and J.D. Cawley, "Intermediate Temperature Strength Degradation in SiC/SiC Composites," *Journal of the European Ceramic Society* 22 2777-2787 (2002).
8. W. Xu, F.W. Zok and R. McMeeking, "Model of Oxidation-Induced Fiber Fracture in SiC/SiC Composites," *J. Am. Ceram. Soc.* 1-8 (2014).
9. P. Forio, F. Lavaire and J. Lamon, "Delayed Failure at Intermediate Temperatures (600 – 700 °C) in Air in Silicon Carbide Multifilament Tows," *J. Am. Ceram. Soc.* 87 [5] 888-893 (2004).
10. W. Gauthier, F. Pailler, J. Lamon and R. Pailler, "Oxidation of Silicon Carbide Fibers During Static Fatigue in Air at Intermediate Temperatures," *J. Am. Ceram. Soc.* 92 [9] 2067-2073 (2009).
11. W. Gauthier and J. Lamon, "Delayed Failure of Hi-Nicalon and Hi-Nicalon S Multifilament Tows and Single Filaments at Intermediate Temperatures (500 °C – 800 °C)," *J. Am. Ceram. Soc.* 92 [3] 702-709 (2009).
12. R.W. Davidge, J.R. McLaren and G. Tappin, "Strength-Probability-Time (SPT) Relationships in Ceramics," *Journal of Materials Science* 8 1699-1705 (1973).
13. J. Aveston, G.A. Cooper and A. Kelly, "Single and Multiple Fracture," pp. 15-26 in the Properties of Fiber Composites, Conference Proceedings of the National Physical Laboratory. IPC Science and Technology Press Ltd. Surrey, England, 1971.
14. W.A. Curtin, "Theory of Mechanical Properties of Ceramic Matrix Composites," *J. Am. Ceram. Soc.*, 74 [11] 2837-45 (1991).
15. M.D. Thouless and A.G. Evans, "Effects of Pull-out on the Mechanical Properties of Ceramic-Matrix Composites," *Acta metall.* 36 [3] 517-522 (1988).
16. M.D. Thouless, O. Sbaizero, L.S. Sigl and A.G. Evans, "Effect of Interface Mechanical Properties on Pullout in a SiC-Fiber-Reinforced Lithium Aluminum Silicate Glass-Ceramic," *J. Am. Ceram. Soc.* 72 [4] 525-32 (1989).
17. W.A. Curtin, "In-situ Fiber Strengths in Ceramic Matrix Composites from Fracture Mirrors," *J. Am. Ceram. Soc.* 77 [4] 1075-78 (1994).
18. W.A. Curtin, B.K. Ahn and N. Takeda, "Modeling Brittle and Tough Stress-Strain Behavior in Unidirectional Ceramic Matrix Composites," *Acta mater.* 46 [10] 3409-3420 (1998).
19. H.G. Halverson and W.A. Curtin, "Stress Rupture in Ceramic Matrix Composites: Theory and Experiment," *J. Amer. Ceram. Soc.*, 85 [6] 1350-65 (2002).
20. W. Weibull, "A Statistical Distribution Function of Wide Applicability," *Journal of Applied Mechanics*, 293-297 (1951).
21. A.C. Kimber and J.G. Keer, "On the Theoretical Average Crack Spacing in Brittle Matrix Composites Containing Continuous Aligned Fibers," *Journal of Materials Science Letters*, 1 353-354 (1982).
22. D.B. Marshall and A.G. Evans, "Failure Mechanisms in Ceramic Fiber/Ceramic Matrix Composites," *J. Amer. Ceram. Soc.*, 68 [5] 225-31 (1985).